Fabrication and rejuvenation of high quantum efficiency caesium telluride photocathodes for high brightness and high average current photoinjectors

M. Martinez-Calderon,[1,*] E. Chevallay,[1] R. E. Rossel,[1] L. B. Jones,[2,3] G. Zevi Della Porta,[1] B. Marsh,[1] and E. Granados[1,†]

[1]*CERN, European Organization for Nuclear Research, 1211 Geneva, Switzerland*
[2]*ASTeC, STFC Daresbury Laboratory, Warrington, United Kingdom*
[3]*Cockcroft Institute of Accelerator Science, Daresbury, United Kingdom*

(Received 20 October 2023; accepted 22 January 2024; published 8 February 2024)

With their high quantum efficiency (QE) and excellent photoemissive properties, cesium telluride (Cs-Te) photocathodes are the current workhorse in the high average current electron accelerators around the globe. Their ability to generate high brightness and high charge electron beams has opened the doorway to numerous applications, including fundamental particle physics research, radiation therapy, high-energy physics experiments, and high repetition rate free-electron lasers (FELs). Their long-term performance is critical. In this work, we analyze the systematic production and rejuvenation of photocathodes via thermal evaporation and deposition techniques (both sequential and co-deposition), showing excellent values of QE exceeding 20% using deep ultraviolet illumination ($\lambda = 262$–266 nm). To extend the photocathode lifetime, the rejuvenation process is performed via multilayer thin-film co-deposition, demonstrating the feasibility of reliably recovering the initial QE even after air exposure. We evaluated their final performance in both high gradient dc and rf gun setups and obtained consistent results of QE and lifetimes. The technique can be used *in situ* at the gun level, which significantly extends the sustained accelerator operation without major interventions. These approaches significantly enhance the robustness and performance of Cs-Te photoinjectors and represent a significant advancement for reliable high average current electron accelerators and FELs.

DOI: 10.1103/PhysRevAccelBeams.27.023401

I. INTRODUCTION

The advancement of the photocathode technology is critical for a multitude of advanced lepton accelerator applications. High brightness and high current electron beams are particularly necessary for hadron cooling [1], high average power x-ray free electron lasers (FELs) [2,3], FEL-based extreme ultraviolet lithography machines [4], γ-ray sources [5], electron diffraction microscopy [6,7] or FLASH radiation therapy [8], and among many others. In these applications, the electron bunch charge and brightness are to some extent determined by the photocathode characteristics and the electric field applied to its surface [9].

Traditionally, the photoemission from metallic surfaces has been widely utilized for electron bunch generation in accelerators. The main advantages are in their robustness and their overall lifetime. However, their low quantum efficiency (QE)—of the order of 10^{-5}—limits significantly the average current achievable in RF photoinjectors [10]. The limitation is mainly caused by a combination of metal damage threshold and stringent requirements for laser average power. For these reasons, next generation photoinjectors used in the high performance electron accelerators, such as the recently commissioned high repetition rate FELs [11,12] are equipped with semiconductor photocathodes. Recently, plasmonic photocathodes have shown promise as a viable alternative solution by enhancing the QE of metallic substrates by orders of magnitude [13–15], although their performance in accelerators remains to be seen.

High QE semiconductor thin films enable the production of high bunch charge and high average current simultaneously with moderate laser requirements, and depending on the choice of material they can operate at convenient wavelengths in the visible and near-IR spectral range [16,17]. Compared to metallic photocathodes, they present a QE many orders of magnitude superior (with QE of up to 20% and beyond). Unfortunately, they are chemically highly reactive, which imposes demanding ultra high-vacuum (UHV) conditions in the 10^{-9} mbar range and

*miguel.martinez.calderon@cern.ch
†eduardo.granados@cern.ch

below [18]. Cesium telluride is perhaps the most widely used semiconductor due to its balanced characteristics in terms of high QE, relatively long lifetime, and resistance to chemical contamination compared to other similarly performing semiconductors.

The main causes of QE degradation include electric breakdowns, contamination with oxygen and other chemical species (mainly CO_2 and H_2O), and laser induced damage to the thin film. When the Cs-Te thin films are degraded, their replacement inevitably requires in-vacuum exchange, which can result in operational interruptions for an accelerator complex. An alternative to photocathode replacement is rejuvenation, a topic that has been poorly studied but can provide a viable pathway to extend the sustained operation of the accelerator. Previous attempts included the cleaning of metallic photocathodes with laser or hydrogen beams [19,20], or heating the photocathode substrate to around 150–200 °C [21], which redistributes the Cs due to diffusion while being illuminated with deep ultraviolet (DUV) light [22]. An interesting alternative for extending the lifetime consists of protecting the photoemissive layer with additional thin films, such as graphene [23–25]), which has shown promising results but complicates further the fabrication process.

Most Cs-Te photocathodes reported in the literature were produced by sequential thermal evaporation and deposition of Te and Cs following the recipe proposed by Di Bonna *et al.* [26]. This recipe results in a reliable QE ranging from 5% to 10% under DUV illumination [27–31]. In contrast, the co-deposition process involves the formation of Cs-Te molecules in the gas phase before their subsequent deposition onto the metallic substrate [32]. This technique is more complex since it requires accurate and real-time monitoring of the QE as well as Cs and Te flow rates during production to achieve the optimal stoichiometry ratio between elements. The advantage, however, is that this process often results in higher QE and lower thin-film roughness [33–35]. Lower roughness further improves the intrinsic emittance and ultimately facilitates the enhancement of the electron beam brightness [36,37]. It is worth mentioning that epitaxial thin-film growth techniques may be beneficial for Cs-Te photocathode preparation, as it has been already shown for alkali-antimonide photocathodes [38].

Cs-Te photocathodes are usually prepared using evaporators of Cs and Te as shown in Fig. 1(a). With this setup, we investigate two different approaches to rejuvenate photocathodes: First, the rejuvenation by producing new co-deposited Cs-Te photoemissive layers on top of the degraded ones [Fig. 1(b)], a technique explored for the first time to the best of our knowledge in this work. Second, the rejuvenation by sequential deposition over multiple Cs-Te layers by adding a 15 nm layer of Te followed by 40 nm of Cs [Fig. 1(c)], a strategy that has been performed *in situ* at the gun level multiple times at the CERN

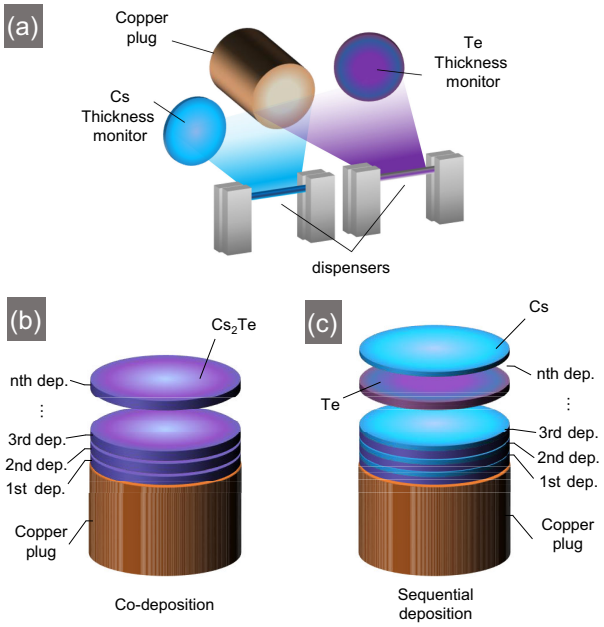

FIG. 1. (a) Typical arrangement of Cs and Te dispensers and quartz microbalances (thickness monitoring) for Cs-Te production via co-deposition. (b) Rejuvenation strategy via co-deposition of Cs-Te photoemissive layers over degraded ones. (c) Rejuvenation strategy via sequential deposition where a new Te layer is deposited on top of the degraded Cs-Te film followed by a new Cs layer.

CLEAR facility [39]. We measured the performance of both approaches in terms of maximum achievable QE.

II. Cs-Te CO-DEPOSITION

For the co-deposition experiments, the Cs-Te photocathodes were prepared at the CERN Photoemission Laboratory in a custom-made preparation chamber under UHV conditions (maintained under 10^{-10} mbar, reached after a typical bake-out procedure starting from air pressure). At room temperature, Cs and Te are known to form a variety of stable Cs_xTe_y compounds. In this paper, we designate generally these compounds as Cs-Te, independently of their stoichiometry ratio. The substrate consisted of a 19-mm diameter top surface oxygen-free electronic grade copper plug (oxygen content $< 0.0005\%$) polished to a surface roughness of Ra < 0.02 μm.

The preparation chamber is equipped with Cs and Te dispensers, which can be simultaneously powered for thermal co-deposition and two quartz microbalances for *in situ* thickness monitoring, equidistant from the dispensers, and the plug surface (partially shielded from each other for quasi-independent thickness reading of each material). However, since the deposited thicknesses were not calibrated during the experiments, the values reported here are the best estimates. At the evaporation position, the photocathode plug is mounted into a receptacle equipped with an rf-oven, which serves for substrate heating (although the

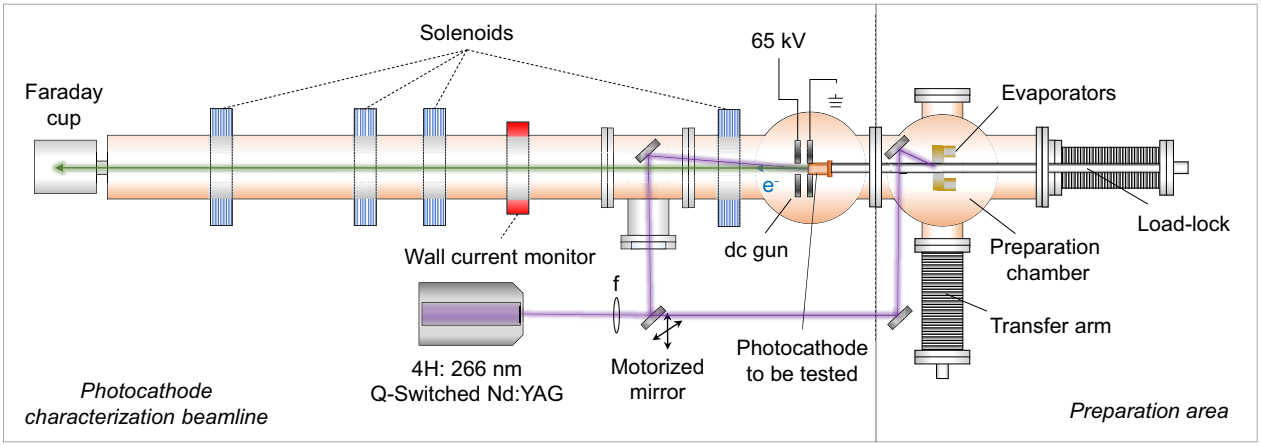

FIG. 2. Schematic layout of the CERN Photoemission Laboratory setup including a preparation area where the Cs-Te photocathodes are produced via co-deposition and a characterization beamline for electron beam acceleration with a dc photoelectron gun.

Cs-Te photocathodes presented here were produced at room temperature) and is surrounded by a circular anode biased at 1 kV with respect to the plug surface. The anode allows for real-time monitoring and optimization of the generated photocurrent (and relative QE) during the co-deposition process, driven by a DUV ($\lambda = 266$ nm) nanosecond pulse laser beam. The produced photocurrent and driving laser pulse energy are continuously monitored in every single shot. A schematic of the preparation area is shown in Fig. 2.

The first step of the production process consists of ramping up the Te dispenser power supply until an evaporation rate of around 0.1 nm/min is reached. This rate is kept constant for the remaining of the growth process. Next, the Cs dispenser power supply is ramped up immediately after Te evaporation rate is fixed. Once Cs starts to be evaporated, the flow rate is progressively increased by manually adjusting the power applied to the dispenser, trying to maximize the generated photocurrent and therefore the relative QE. Figure 3 displays the relationship between the Cs-Te estimated stoichiometric deposition ratio and the relative QE for two fresh Cs-Te [identified as photocathodes (A) and (B)] as well as their rejuvenation using the co-deposition technique. The stoichiometric deposition ratio η was estimated using the following equation:

$$\eta = \frac{\rho(\mathrm{Cs})t(\mathrm{Cs})m(\mathrm{Te})}{\rho(\mathrm{Te})t(\mathrm{Te})m(\mathrm{Cs})}, \tag{1}$$

where ρ and m are the material density and atomic mass, respectively, and t the tellurium and cesium deposited thicknesses, which were estimated from the raw data taking into account the microbalances crosstalk and their accuracy. The relative production QE values displayed in the plot were scaled appropriately after measuring the QE with the dc gun characterization beamline depicted in Fig. 2. Right after fabrication, the plugs were directly transferred to the beamline and consecutive QE measurements verified that the performance was not degraded during transport from one chamber to the other one within the setup. The acceleration of electron bunches was produced with a potential of 65 kV which led to an electric field amplitude of 6.5 MV/m at the photocathode surface. To drive the photoemission process, a linearly polarized DUV laser beam at $\lambda = 266$ nm, 5 ns pulse duration, and 10 Hz repetition rate was directed to the active photocathode surface via an in-vacuum mirror with an incidence angle of 5° with respect to the surface normal. Four solenoids provided focusing along the electron beamline, and the electron bunch charge was monitored simultaneously by a wall-current monitor and a Faraday cup.

In the case of photocathode (A), the QE moderately increases for a relatively low Cs-Te stoichiometric

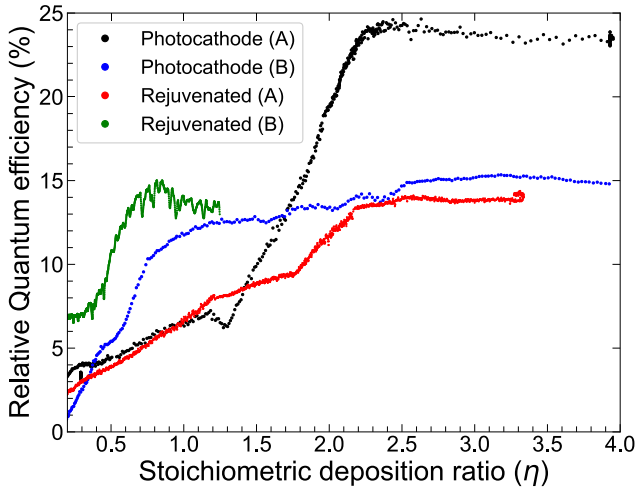

FIG. 3. Evolution of the relative QE measured during the co-deposition fabrication process of Cs-Te photoemissive layers as a function of the Cs-Te estimated stoichiometric deposition ratio under DUV laser illumination ($\lambda = 266$ nm).

deposition ratio of 1 and then exhibits a prominent increase for a higher Cs-Te ratio. The Te rate was set to a fixed value of 0.07 nm/min. For a stoichiometric deposition ratio slightly above 2, the QE is clamped at its maximum value, reaching a value of almost 25%, which is one of the highest reported to date using DUV laser wavelength. The total accumulated thickness of Cs and Te thin films were 43.7, and 3.24 nm, respectively, leading to a final estimated stoichiometric deposition ratio of almost 4. However, the measurement results show that an estimated ratio of 2.3 was optimal to maximize the QE.

In the case of photocathode (B), a similar approach was followed, but slightly higher Te and Cs evaporation rates were employed (fixed at 0.12 nm/min for Te), leading therefore to a steeper increase in the stoichiometric deposition ratio. The QE value showed a prominent growth to 12% when a Cs-Te ratio of 1 was reached, but when the ratio was further increased, the slope was diminished considerably to finally stabilize at a QE value of 16%. For this photocathode growth conditions, the total accumulated Cs and Te thicknesses were 59.2 and 4.26 nm, respectively, leading again to a final stoichiometric deposition ratio nearly of 4. This fabrication process also evidences that a stoichiometric deposition ratio higher than 2.3 does not suppose any advantage in terms of maximizing the QE.

A. Rejuvenation process

After fresh production, both photocathodes (A) and (B) were used at CERN's AWAKE experiment rf gun for different periods of time. The transport after fabrication was performed using a custom transport carrier vacuum vessel, which ensured photocathode storage under UHV conditions (pressure $< 10^{-10}$ mbar). Both photocathodes were stored for approximately 4 years before being deployed at AWAKE. Photocathode (A) was used for 9 months before being accidentally exposed to air. Photocathode (B) was used for 2 years until it was replaced and stored in the transport carrier under UHV. Both photocathodes were transported back to the CERN Photoemission Laboratory where the rejuvenation process was conducted.

Before starting the rejuvenation process, the QE of both photocathodes was measured in the characterization beamline, similar to when they were newly prepared. Photocathode (A) QE was measured to be $<0.01\%$, confirming that the air exposure greatly degraded the photoemissive layer. This QE is similar to that of bare copper. The used photocathode (B) QE was found to be degraded down to 0.16% probably due to continuous use. The specific factors leading to degradation might include contamination with oxygen and other chemical species, laser induced damage, or the formation of metallic Te clusters [17,40].

In the case of photocathode (A), it was attempted to exactly replicate the highly successful original fabrication process leading to a QE of 25%. However, the Te evaporation rate during the rejuvenation was fixed to an excessively high rate of 0.12 nm/min, and consequently, the Cs deposition rate required to maintain an optimal stoichiometric deposition ratio was hard to control precisely. Figure 3 shows that while the first part of the growth exhibited a similar trend up to a stoichiometry ratio of approximately 1, further increasing the ratio did not produce the same QE increase as in the original fabrication and the maximum obtained was 14%. The total accumulated Te and Cs thicknesses were 62 and 5.59 nm, respectively, while the final stoichiometric deposition ratio was 3.27. Again, the QE was clamped to its maximum value once the ratio of 2.3 was reached. For photocathode (B), the initial conditions for rejuvenation were different since the Cs-Te photoemissive layer was still present. The measurement of the QE before rejuvenation yielded a value of QE $\approx 0.2\%$, and it is assumed that it was never exposed to any contaminants. Here with significantly less evaporation of Cs, we were able to recover up to 95% of its original QE with a stoichiometric deposition ratio of 1.24, also shown in Fig. 3. Table I presents a summary of the main growth parameters and photoemissive performance for each photocathode initial fabrication and rejuvenation.

B. QE spatial homogeneity

To spatially characterize the homogeneity of the fresh and rejuvenated cathodes, the DUV laser beam was focused to a spot size of approximately 2 mm (FWHM) onto the surface of the photocathode and rastered using a motorized mirror while simultaneously measuring the generated charge, thus allowing QE mapping. The spatial QE analysis of fresh photocathodes (A) and (B) is presented in Figs. 4(a) and 4(b). The measurements showed that photocathode (A) performed better in terms of QE

TABLE I. Summary of fabrication and QE for photocathodes (A) and (B) before use and after rejuvenation.

	Fixed Te rate (nm/min)	Te thickness (nm)	Cs thickness (nm)	Stoichiometry ratio	Max. QE (%)
Photocathode (A)	0.07	3.24	43.7	3.93	25
Photocathode (B)	0.12	4.26	59.2	3.91	16
Rejuvenated (A)	0.12	5.59	62	3.27	14
Rejuvenated (B)	0.12	5.17	22.8	1.24	15

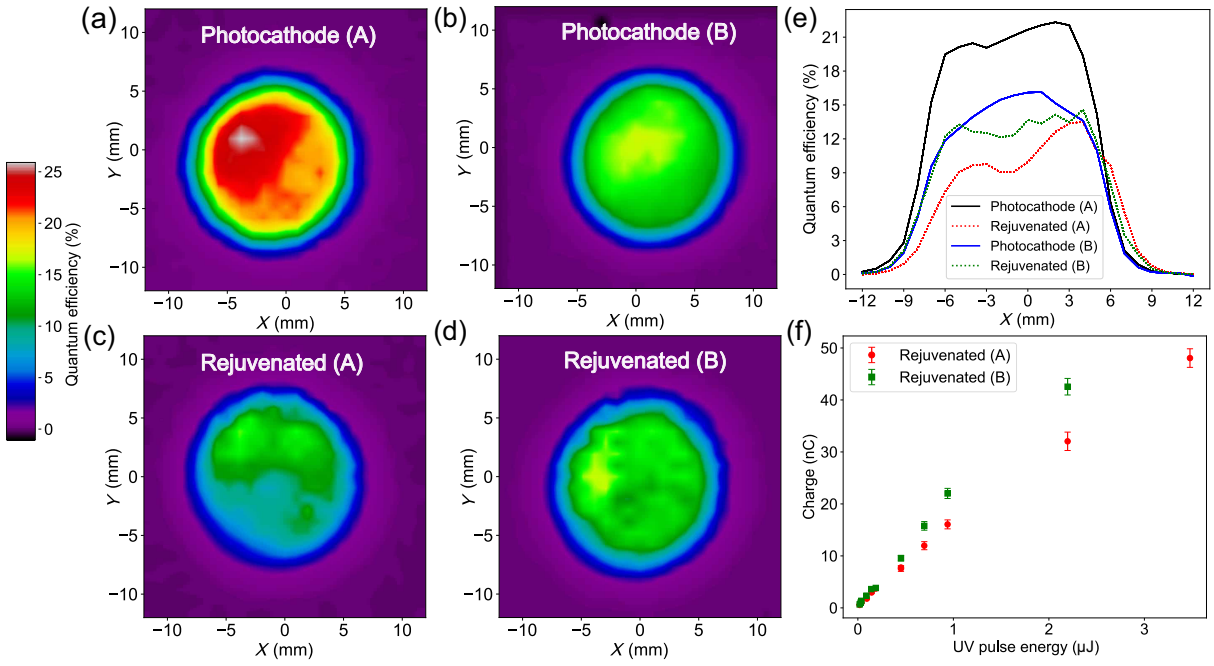

FIG. 4. 2D colormaps showing the distribution of the measured QE over the surface of: (a) fresh photocathode (A) using a pulse energy ($\lambda = 266$ nm) of 58 nJ, (b) fresh photocathode (B) at 66 nJ, (c) rejuvenated photocathode (A) at 37 nJ, and (d) rejuvenated photocathode (B) at 187 nJ. (e) Averaged line-outs extracted from the QE maps for the values measured in a section of $X = \pm 2$ mm. (f) Photoemissive behavior analysis showcasing the electron beam charge as function of the UV pulse energy measured for the rejuvenated photocathodes (A) and (B) in the dc gun characterization beamline. The QE maps were obtained at a resolution of one data point per mm^2 area, while each data point consisted of 20 consecutive readings of the electron beam charge measured with the wall current monitor acquired at a laser repetition rate of 10 Hz.

(showing a maximum QE up to 25% at 58 nJ UV pulse energy). Photocathode (B) showed an original QE of about 16% at 66 nJ pulse energy and displayed a highly homogeneous QE spatial distribution. Compared to the Cs-Te photocathodes reported in the literature (where the typical maximum QE is around 10%), the performance of both (A) and (B) photocathodes could be considered outstanding and matching well the optimum expected values for co-evaporated Cs-Te [33].

The QE characterization of the rejuvenated photocathodes is shown in Figs. 4(c) and 4(d). The rejuvenated photocathode (A) presented a maximum QE of 14% which represents a 56% of its initial QE value but with a rather inhomogenous QE spatial distribution. In the case of the rejuvenated photocathode (B), it can be observed that a QE of up to 15% was measured and therefore 95% of the original QE was restored through the rejuvenation process. The overall QE spatial distribution retrieved exhibits a higher degree of uniformity compared to that of the rejuvenated photocathode (A). Figure 4(e) shows averaged line-outs of a 4 mm control band across the surface of the QE extracted from the 2D maps to allow a comparison between the produced photocathodes before and after rejuvenation. The charge produced at the center of the photocathode as a function of impinging DUV pulse energy is presented in Fig. 4(f), where it is shown that a very high bunch charge of up to 50 nC could be easily obtained with the rejuvenated photocathodes under μJ pulse energy illumination.

C. Performance in an rf gun

As described before, subsequent to their initial fabrication and characterization, the photocathodes have been used at the AWAKE experiment rf photoelectron gun [41]. The gun is equipped with a load-lock system to load the UHV transport carrier and insert the photocathodes produced at the Photoemission Laboratory. The photoinjector consists of an S-band rf gun and a traveling wave booster structure producing electron beams with an energy of 16–20 MeV (using a 3 GHz, 2.5-cell rf gun and a 1-m-long booster structure [42]. The maximum accelerating gradient is set to 79.6 MV/m at the photocathode surface to accelerate the electron bunches to an energy of 5.3 MeV out of the rf gun [43].

The electron bunch generation in the rf gun is driven by a UV beam generated by the AWAKE main laser system, which comprises a mode-locked fiber laser oscillator locked to an rf reference, a pulse stretcher, a series or Ti:Sapphire multipass amplifiers, and two separate grating pulse compressors (one dedicated to the ionizing beam and a second one for generating the UV pulses for electron beam production). A small fraction of the initial laser power

is frequency tripled to a wavelength of 262 nm and sent via an off-axis mirror to the photocathode surface at a repetition rate of 10 Hz, with energy up to 10 μJ and a variable pulse duration which in most of the experiments was set to 1.2 ps (FWHM) [42].

Figure 5 shows the commissioning results of photocathode (A) at AWAKE in March 2023, showcasing a QE up to 25% at low charges (UV energies below 15 nJ) and therefore limited space-charge effects. The QE is usually lower than the nominal maximum QE as it is subjected to saturation and space-charge effects, while in optimal conditions they would be approximately equal. Under saturation conditions (i.e., UV pulse energies higher than 15 nJ, which correspond to fluences higher than approximately 1.3 $\mu J/cm^2$), the QE was measured to be well above 12% as shown in Fig. 5(b). Photocathode (B) commissioning results at AWAKE rf gun showed a maximum measured QE of 12%, which then decayed down to less than 1% after 2 years of heavy use. The commissioning results show that the QEs at AWAKE are well matched to the QE measured with the dc gun.

Apart from the QE, the emittance of both photocathodes was analyzed multiple times during the AWAKE experiment runs [44,45]. The best emittance results were obtained with each photocathode when using the typically needed bunch charge of 300 pC, UV pulse energy of 100 nJ, and a laser beam spot size of 300 μm, yielding a normalized emittance value of less than 1 mm mrad for an electron bunch energy of 5.5 MeV. The bunch duration was estimated to be around 2 ps [42].

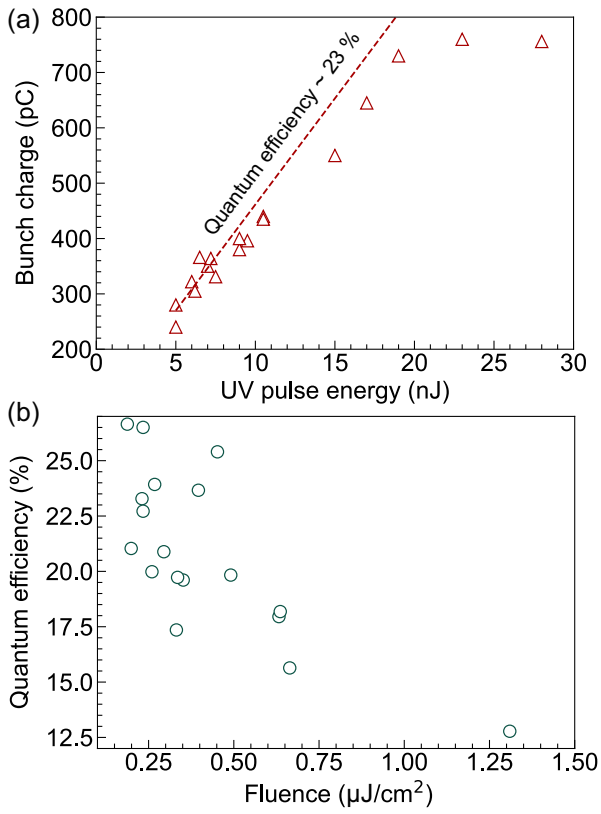

FIG. 5. (a) Characterization of the electron beam generation at AWAKE experiment rf gun showing the bunch charge as function of the UV pulse energy ($\lambda = 262$ nm) delivered to the photocathode surface and (b) the measured quantum efficiency as function of the laser fluence for the fresh photocathode (A), surpassing 25%.

III. *IN SITU* SEQUENTIAL DEPOSITION

The second strategy for Cs-Te rejuvenation has been carried out *in situ* at the gun level in the CLEAR facility at CERN during the last 6 years. Here the photoinjector is equipped with an independent vacuum section behind the gun that can be isolated. This dedicated chamber includes Cs and Te dispensers as shown in Fig. 6. The Cs-Te photocathode is produced in a so-called *blind deposition* since there is no QE online monitoring. The deposited thickness of each element can be monitored with a single quartz microbalance. The fresh fabrication followed the standard recipe proposed by di-Bona *et al.* [26] and consisted of the deposition of a Te 15 nm film followed by a 40 nm Cs film. The rejuvenation processes consisted of repeating the same sequential deposition on top of the used Cs-Te photoemissive layer. No substrate heating was performed during the sequential depositions. The sequentially deposited photocathodes are used at CLEAR CERN facility, which consists of an S-band rf photoinjector and three S-band accelerating structures followed by a 20 m long experimental beamline [46]. The electron bunch is driven by a UV beam produced by a home-built all-solid-state Nd:YLF system. This laser system is composed of oscillator and preamplifier, main amplifier, and frequency

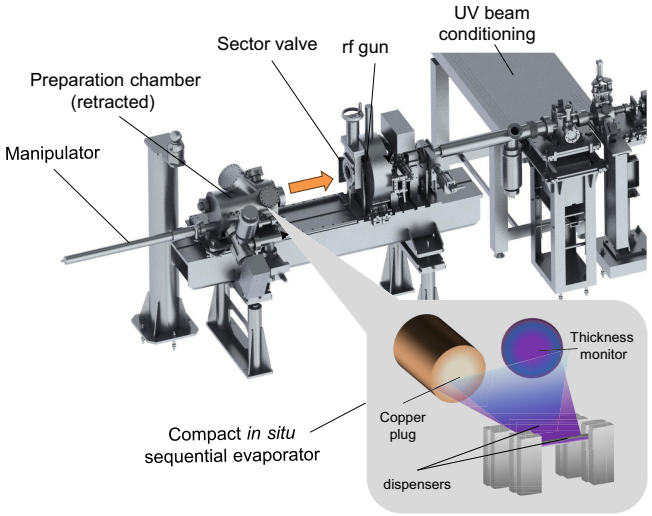

FIG. 6. Computer aided rendering of the CLEAR accelerator photoinjector showing the retractable preparation chamber where *in situ* rejuvenation is performed. Inset: Illustrative scheme of the miniature evaporators for the rejuvenation processes carried out in the copper photocathode plug.

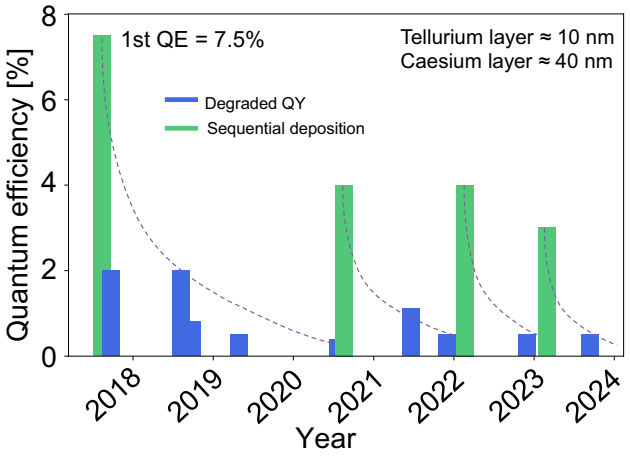

FIG. 7. Yearly evolution of the QE at CERN's CLEAR facility after the initial fresh sequentially deposited Cs-Te photocathode and three consecutive rejuvenations carried out when the QE was measured to be below 0.5%.

quadrupling stage. The UV laser source is centered at $\lambda = 262$ nm, with a laser pulse energy up to 1.5 μJ per pulse, pulse duration of 4.7 ps, and variable repetition rate from 0.83 to 10 Hz [47].

The achieved rejuvenated QE results are presented in Fig. 7. The initial QE of 7.5% decayed with use down to 0.5% after almost 3 years of operation. At that point, the first rejuvenation was carried out and the measured QE was restored to a value of 4%, which decayed again to about 0.5% after 1 year of intense use. Similar trends were observed with the subsequent rejuvenation processes carried out until today, when the operation of the CLEAR facility is 24/7. The typical amount of integrated charge extracted from each rejuvenated cathode is as much as 1 Coulomb over 1000 of hours of use. The decay rate of the QE is difficult to estimate since the experiments occurring at the CLEAR facility use widely different electron beam configurations, such as variable laser spot size illumination, pulse energy, repetition rate, resulting bunch charge, and number of bunches per train.

IV. DISCUSSION AND CONCLUSIONS

In summary, we reported on the production of co-deposited and sequential Cs-Te photocathodes exhibiting high QE, and their successful operation in dc and rf photoelectron guns at CERN accelerators, where they constitute the electron source. The fabrication results show that with the current fabrication setup, the deviation in terms of resulting QE is significant but reliably over 15%. We found that from the fabrication data are possible to estimate an optimal stoichiometric deposition ratio and corresponding evaporation rate, which leads to the reproducible fabrication of high QE Cs-Te photocathodes. Furthermore, we determined that not only the final stoichiometric deposition ratio determines the QE, but also the dynamic evaporation rates of Cs and Te are crucial. In particular, it was found that during the production of photocathode (A) (which showed the highest QE), the main difference was a lower fixed Te evaporation rate and the final photoemissive thin-film layer thickness. We show that further increasing the Cs:Te ratio did not affect the performance of the photocathodes in terms of maximum achievable QE, but it might have consequences in the emittance or lifetime of the photocathodes. These results point at avenues for further optimization, which should include a thorough study of the impact of lower growth rates and final thickness on the Cs-Te photocathodes QE and lifetime.

As an alternative to co-deposition, we presented the strategy of *in situ* rejuvenation via Cs-Te sequential deposition at the gun level performed at the CLEAR facility at CERN, which allowed sustained operation of the photocathode for the last 6 years showcasing continuous reliable QE recovery values well over 1%. The QE reached using this growth method is significantly lower when compared to the co-deposition technique, but it is far simpler and easier to implement at the gun level, resulting in extremely useful sources for accelerator sustained operation.

It is complicated to ultimately determine the chemical composition of the produced Cs-Te thin films at the production stage. Most of the studies analyzing the Cs-Te composition concluded that the final chemical composition often consists of random combinations of different Cs_xTe_y, which leads to a wide variability in the achieved QE and resulting lifetime [28,33]. The comparatively high QE results presented here are in line with the recent work of Cocchi *et al.* [48], where a predominant Cs_2Te electronic structure is necessary for achieving high QE. The growth data rendered an optimum stoichiometric deposition ratio of 2.3, although the exact chemical composition of the thin film is unknown. Future spectroscopy studies of co-deposited Cs-Te and advanced computational methods of Cs-Te binary system are key to keep advancing on establishing this technology as the most reliable source for the future electron accelerators [49].

In practical terms, we show that the photocathode rejuvenation is a viable solution. We presented for the first time (to the best of our knowledge) an approach for in-vacuum rejuvenation of Cs-Te via co-deposition. The results show that it is feasible to recover initial high QE after heavy use or even air vacuum accidental exposure. Interestingly, we found that for the photocathode exposed to air, the QE could be restored to about 60% of its initial value (even with nonideal fabrication parameters), whereas for a simply used photocathode, the QE was recovered to about a 95%.

A summary of the overall performance of fresh and rejuvenated photocathodes via co-deposition is presented in Table II. It should be noted that after analyzing the data,

TABLE II. Summary of photocathodes performance before and after rejuvenation.

Co-deposition	QE (%)	e gun
Fresh (A)	25/23	dc gun/rf gun
Degraded (A)	0.01	dc gun
Rejuvenated (A)	14	dc gun
Fresh (B)	16/12	dc gun/rf gun
Degraded (B)	0.16	dc gun
Rejuvenated (B)	15	dc gun
Sequential		
First deposition (2018)	7.5	rf gun
Second deposition (2021)	~4	rf gun
Third deposition (2022)	~4	rf gun
Fourth deposition (2023)	~3	rf gun

the rejuvenation process of photocathode (A) showed a similar trend as the fresh fabrication of photocathode (B) which did not result in the highest QE. We believe that the rejuvenation via co-deposition of photocathode (A) could have yielded an even higher QE than reported here, mainly because the growth conditions were not optimal in terms of Te growth rate. Conversely, the rejuvenated Cs-Te photocathodes showed a decrease in QE spatial homogeneity across the surface, probably due to the insertion of contaminants. Postmortem analysis of the surface composition and roughness of the rejuvenated photocathodes will be realized to understand their effect on the final performance. The rejuvenation results presented in this work open the door to future photoinjector designs including the capability of *in situ* rejuvenation of Cs-Te photocathodes via co-deposition technique allowing for the best output in terms of maximum QE.

[1] A. V. Fedotov *et al.*, Experimental demonstration of hadron beam cooling using radio-frequency accelerated electron bunches, Phys. Rev. Lett. **124**, 084801 (2020).

[2] E. Prat *et al.*, A compact and cost-effective hard x-ray free-electron laser driven by a high-brightness and low-energy electron beam, Nat. Photonics **14**, 748 (2020).

[3] P. Emma *et al.*, First lasing and operation of an ångstrom-wavelength free-electron laser, Nat. Photonics **4**, 641 (2010).

[4] Y. Socol, G. N. Kulipanov, A. N. Matveenko, O. A. Shevchenko, and N. A. Vinokurov, Compact 13.5-nm free-electron laser for extreme ultraviolet lithography, Phys. Rev. ST Accel. Beams **14**, 040702 (2011).

[5] F. Albert, S. G. Anderson, D. J. Gibson, R. A. Marsh, S. S. Wu, C. W. Siders, C. P. J. Barty, and F. V. Hartemann, Design of narrow-band compton scattering sources for nuclear resonance fluorescence, Phys. Rev. ST Accel. Beams **14**, 050703 (2011).

[6] D. Filippetto, P. Musumeci, R. K. Li, B. J. Siwick, M. R. Otto, M. Centurion, and J. P. F. Nunes, Ultrafast electron diffraction: Visualizing dynamic states of matter, Rev. Mod. Phys. **94**, 045004 (2022).

[7] J. B. Hastings, F. M. Rudakov, D. H. Dowell, J. F. Schmerge, J. D. Cardoza, J. M. Castro, S. M. Gierman, H. Loos, and P. M. Weber, Ultrafast time-resolved electron diffraction with megavolt electron beams, Appl. Phys. Lett. **89**, 184109 (2006).

[8] L. Whitmore, R. I. Mackay, M. van Herk, J. K. Jones, and R. M. Jones, Focused VHEE (very high energy electron) beams and dose delivery for radiotherapy applications, Sci. Rep. **11**, 14013 (2021).

[9] I. V. Bazarov, B. M. Dunham, and C. K. Sinclair, Maximum achievable beam brightness from photoinjectors, Phys. Rev. Lett. **102**, 104801 (2009).

[10] C. J. Knill, S. Douyon, K. Kawahara, H. Yamaguchi, G. Wang, H. Ago, N. Moody, and S. Karkare, Effects of nonlinear photoemission on mean transverse energy from metal photocathodes, Phys. Rev. Accel. Beams **26**, 093401 (2023).

[11] F. Zhou, C. Adolphsen, D. Dowell, and R. Xiang, Overview of CW electron guns and LCLS-II RF gun performance, Front. Phys. **11** (2023).

[12] E. Sobolev, Megahertz single-particle imaging at the european XFEL, Commun. Phys. **3**, 97 (2020).

[13] C. M. Pierce, D. B. Durham, F. Riminucci, S. Dhuey, I. Bazarov, J. Maxson, A. M. Minor, and D. Filippetto, Experimental characterization of photoemission from plasmonic nanogroove arrays, Phys. Rev. Appl. **19**, 034034 (2023).

[14] A. Polyakov, C. Senft, K. F. Thompson, J. Feng, S. Cabrini, P. J. Schuck, H. A. Padmore, S. J. Peppernick, and W. P. Hess, Plasmon-enhanced photocathode for high brightness and high repetition rate x-ray sources, Phys. Rev. Lett. **110**, 076802 (2013).

[15] M. Martinez-Calderon, B. Groussin, V. Bjelland, E. Chevallay, V. N. Fedosseev, M. Himmerlich, P. Lorenz, A. Manjavacas, B. A. Marsh, H. Neupert, R. E. Rossel, W. Wuensch, and E. Granados, Hot electron enhanced photoemission from laser fabricated plasmonic photocathodes, Nanophotonics (2023), 10.1515/nanoph-2023-0552

[16] H. Panuganti, E. Chevallay, V. Fedosseev, and M. Himmerlich, Synthesis, surface chemical analysis, lifetime studies and degradation mechanisms of CS-K-SB photocathodes, Nucl. Instrum. Methods Phys. Res., Sect. A **986**, 164724 (2021).

[17] J. Schaber, R. Xiang, and N. Gaponik, Review of photocathodes for electron beam sources in particle accelerators, J. Mater. Chem. C **11**, 3162 (2023).

[18] D. Dowell, I. Bazarov, B. Dunham, K. Harkay, C. Hernandez-Garcia, R. Legg, H. Padmore, T. Rao, J. Smedley, and W. Wan, Cathode R&D for future light sources, Nucl. Instrum. Methods Phys. Res., Sect. A **622**, 685 (2010).

[19] F. Zhou, A. Brachmann, F.-J. Decker, P. Emma, S. Gilevich, R. Iverson, P. Stefan, and J. Turner, High-brightness electron beam evolution following laser-based cleaning of a photocathode, Phys. Rev. ST Accel. Beams **15**, 090703 (2012).

[20] D. H. Dowell, F. K. King, R. E. Kirby, J. F. Schmerge, and J. M. Smedley, In situ cleaning of metal cathodes using a hydrogen ion beam, Phys. Rev. ST Accel. Beams **9**, 063502 (2006).

[21] S. Kong, D. Nguyen, R. Sheffield, and B. Sherwood, Fabrication and characterization of cesium telluride photocathodes: A promising electron source for the Los Alamos Advanced FEL, Nucl. Instrum. Methods Phys. Res., Sect. A **358**, 276 (1995).

[22] A. di Bona, F. Sabary, S. Valeri, P. Michelato, D. Sertore, and G. Suberlucq, Auger and x-ray photoemission spectroscopy study on Cs_2Te photocathodes, J. Appl. Phys. **80**, 3024 (1996).

[23] J. Biswas, M. Gaowei, A. Liu, S. Poddar, L. Stan, J. Smedley, J. T. Sadowski, and X. Tong, Cesium intercalation of graphene: A 2D protective layer on alkali antimonide photocathode, APL Mater. **10**, 111115 (2022).

[24] L. Guo, F. Liu, K. Koyama, N. Regis, A. M. Alexander, G. Wang, J. DeFazio, J. A. Valdez, A. Poudel, M. Yamamoto, N. A. Moody, Y. Takashima, and H. Yamaguchi, Author correction: Rugged bialkali photocathodes encapsulated with graphene and thin metal film, Sci. Rep. **13**, 3554 (2023).

[25] F. Liu, L. Guo, J. DeFazio, V. Pavlenko, M. Yamamoto, N. A. Moody, and H. Yamaguchi, Photoemission from bialkali photocathodes through an atomically thin protection layer, ACS Appl. Mater. Interfaces **14**, 1710 (2022).

[26] A. di Bona, F. Sabary, S. Valeri, P. Michelato, D. Sertore, and G. Suberlucq, Auger and x-ray photoemission spectroscopy study on Cs2Te photocathodes, J. Appl. Phys. **80**, 3024 (1996).

[27] Z. Yusof, A. Denchfield, M. Warren, J. Cardenas, N. Samuelson, L. Spentzouris, J. Power, and J. Zasadzinski, Photocathode quantum efficiency of ultrathin Cs2Te layers on NB substrates, Phys. Rev. Accel. Beams **20**, 123401 (2017).

[28] C. M. Pierce, J. K. Bae, A. Galdi, L. Cultrera, I. Bazarov, and J. Maxson, Beam brightness from Cs–Te near the photoemission threshold, Appl. Phys. Lett. **118**, 124101 (2021).

[29] D. Sertore, M. Bertucci, G. Guerini Rocco, S. Mohanty, L. Monaco, H. Qian, and F. Stephan, R&D on high QE photocathodes at INFN LASA, in *Proceedings of the 13th International Particle Accelerator Conference, IPAC-2022, Bangkok, Thailand* (JACoW, CERN, Geneva, Switzerland, 2022).

[30] D. Filippetto, H. Qian, and F. Sannibale, Cesium telluride cathodes for the next generation of high-average current high-brightness photoinjectors, Appl. Phys. Lett. **107**, 042104 (2015).

[31] E. Chevallay, J. Durand, S. Hutchins, G. Suberlucq, and M. Wurgel, Photocathodes tested in the dc gun of the CERN photoemission laboratory, Nucl. Instrum. Methods Phys. Res., Sect. A **340**, 146 (1994).

[32] E. Chevallay, Experimental results at the CERN Photoemission Laboratory with co-deposition photocathodes in the frame of the CLIC studies, CERN Internal Note CTF3-Note No. , 2012.

[33] M. Gaowei, J. Sinsheimer, D. Strom, J. Xie, J. Cen, J. Walsh, E. Muller, and J. Smedley, Codeposition of ultrasmooth and high quantum efficiency cesium telluride photocathodes, Phys. Rev. Accel. Beams **22**, 073401 (2019).

[34] C. T. Parzyck, C. A. Pennington, W. J. I. DeBenedetti, J. Balajka, E. Echeverria, H. Paik, L. Moreschini, B. D. Faeth, C. Hu, J. K. Nangoi, V. Anil, T. A. Arias, M. A. Hines, D. G. Schlom, A. Galdi, K. M. Shen, and J. M. Maxson, Atomically smooth films of CsSb: A chemically robust visible light photocathode, arXiv:2305.19553.

[35] A. Galdi, W. J. I. DeBenedetti, J. Balajka, L. Cultrera, I. V. Bazarov, J. M. Maxson, and M. A. Hines, The effects of oxygen-induced phase segregation on the interfacial electronic structure and quantum efficiency of Cs_3Sb photocathodes, J. Chem. Phys. **153**, 144705 (2020).

[36] A. Galdi, J. Balajka, W. J. DeBenedetti, L. Cultrera, I. V. Bazarov, M. A. Hines, and J. M. Maxson, Reduction of surface roughness emittance of Cs_3Sb photocathodes grown via codeposition on single crystal substrates, Appl. Phys. Lett. **118** (2021).

[37] J. Feng, S. Karkare, J. Nasiatka, S. Schubert, J. Smedley, and H. Padmore, Near atomically smooth alkali antimonide photocathode thin films, J. Appl. Phys. **121**, 044904 (2017).

[38] C. T. Parzyck, A. Galdi, J. K. Nangoi, W. J. I. DeBenedetti, J. Balajka, B. D. Faeth, H. Paik, C. Hu, T. A. Arias, M. A. Hines, D. G. Schlom, K. M. Shen, and J. M. Maxson, Single-crystal alkali antimonide photocathodes: High efficiency in the ultrathin limit, Phys. Rev. Lett. **128**, 114801 (2022).

[39] D. Gamba, R. Corsini, S. Curt, S. Doebert, W. Farabolini, G. Mcmonagle, P. Skowronski, F. Tecker, S. Zeeshan, E. Adli, C. Lindstrøm, A. Ross, and L. Wroe, The clear user facility at CERN, Nucl. Instrum. Methods Phys. Res., Sect. A **909**, 480 (2018).

[40] S. Lederer, D. Zeuthen, H. Durr, J. Han, P. Michelato, L. Monaco, R. Ovsyannikov, C. Pagani, S. Schreiber, D. Sertore, M. Sperling, F. Stephan, and A. Vollmer, XPS studies of Cs_2Te photocathodes, in *Proceedings of the 29th International Free Electron Laser conference, Novosibirsk, Russia* (2007), https://accelconf.web.cern.ch/f07/papers/wepph048.pdf.

[41] E. Adli, A. Ahuja, O. Apsimon, R. Apsimon, A.-M. Bachmann, D. Barrientos, F. Batsch, J. Bauche, V. Berglyd Olsen, M. Bernardini *et al.*, Acceleration of electrons in the plasma wakefield of a proton bunch, Nature (London) **561**, 363 (2018).

[42] S.-Y. Kim, S. Doebert, O. Apsimon, R. Apsimon, G. Burt, M. Dayyani, S. Gessner, I. Gorgisyan, E. Granados, S. Mazzoni, J. Moody, M. Turner, B. Williamson, and M. Chung, Commissioning of the electron injector for the awake experiment, Nucl. Instrum. Methods Phys. Res., Sect. A **953**, 163194 (2020).

[43] E. Granados, A.-M. Bachmann, E. Chevallay, S. Döbert, V. Fedosseev, F. Friebel, S. Gessner, E. Gschwendtner, S. Kim, S. Mazzoni, J. Moody, M. Turner, and L. Verra (AWAKE Collaboration), Mapping charge capture and acceleration in a plasma wakefield of a proton bunch using variable emittance electron beam injection, arXiv:2206.14075.

[44] F. M. Velotti, B. Goddard, V. Kain, R. Ramjiawan, G. Z. D. Porta, and S. Hirlaender, Towards automatic setup of

18 mev electron beamline using machine learning, Mach. Learn. **4**, 025016 (2023).

[45] V. Bencini, S. Doebert, E. Gschwendtner, E. Granados, F. Velotti, L. Verra, and G. Zevi Della Porta, Beam characterization and optimisation for AWAKE 18 MeV electron line, in *Proceedings of the 14th International Particle Accelerator Conference, IPAC-2023, Venice, Italy* (JACoW, CERN, Geneva, Switzerland, 2023).

[46] R. Corsini, L. A. Dyks, W. Farabolini, P. Korysko, A. Malyzhenkov, V. Rieker, and K. Sjobak, Status of the CLEAR user facility at CERN and its experiments, in *Proceedings of the 31st Linear Accelerator Conference, LINAC-2022, Liverpool, UK* (JACoW, Geneva, Switzerland, 2022), p. 753.

[47] E. Granados, E. Chevallay, V. Fedosseev, and H. Panuganti (CLEAR), Capabilities and performance of the CLEAR facility photo-injector, CERN, Geneva, Switzerland, Technical Report No. CERN-OPEN-2020-002, 2019.

[48] H.-D. Saßnick and C. Cocchi, Exploring cesium–tellurium phase space via high-throughput calculations beyond semi-local density-functional theory, J. Chem. Phys. **156**, 104108 (2022).

[49] J. Lewellen, D. Filippetto, S. Karkare, J. Maxson, P. Musumeci, J. Smedley, and T. Vecchione, The quest for the perfect cathode, in *Proceedings of the 5th International Particle Accelerator Conference, NAPAC'22, Dresden, Germany* (JACoW, Geneva, Switzerland, 2022), pp. 281–284.